CANCER

DNAzyme Targeting *c-jun* Suppresses Skin Cancer Growth

Hong Cai,[1] Fernando S. Santiago,[1] Leonel Prado-Lourenco,[1] Bo Wang,[1]* Margaret Patrikakis,[1] Miles P. Davenport,[1] Ghassan J. Maghzal,[2] Roland Stocker,[2] Christopher R. Parish,[3] Beng H. Chong,[1] Graham J. Lieschke,[4†] Tak-Wah Wong,[5] Colin N. Chesterman,[1] Douglas J. Francis,[6] Fergal J. Moloney,[7‡] Ross St.C. Barnetson,[7] Gary M. Halliday,[7] Levon M. Khachigian[1§]

Worldwide, one in three cancers is skin-related, with increasing incidence in many populations. Here, we demonstrate the capacity of a DNAzyme-targeting c-*jun* mRNA, Dz13, to inhibit growth of two common skin cancer types—basal cell and squamous cell carcinomas—in a therapeutic setting with established tumors. Dz13 inhibited tumor growth in both immunodeficient and immunocompetent syngeneic mice and reduced lung nodule formation in a model of metastasis. In addition, Dz13 suppressed neovascularization in tumor-bearing mice and zebrafish and increased apoptosis of tumor cells. Dz13 inhibition of tumor growth, which required an intact catalytic domain, was due in part to the induction of tumor immunity. In a series of good laboratory practice–compliant toxicology studies in cynomolgus monkeys, minipigs, and rodents, the DNAzyme was found to be safe and well tolerated. It also did not interfere in more than 70 physiologically relevant in vitro bioassays, suggesting a reduced propensity for off-target effects. If these findings hold true in clinical trials, Dz13 may provide a safe, effective therapy for human skin cancer.

INTRODUCTION

Basal cell carcinoma (BCC) and squamous cell carcinoma (SCC) are two types of skin cancer, which is the most common human cancer (*1*). BCCs form the most prevalent skin tumors, representing about 75% of all skin cancer (*2*, *3*). BCCs rarely metastasize but are locally invasive and can erode and destroy surrounding tissue. Cutaneous SCCs, which make up about 20% of all skin cancers, generally grow faster than BCCs and can metastasize. Current treatment options for BCC and SCC can cause scarring, have low efficacy, or induce side effects that limit their tolerability by patients. Safe and effective alternative treatments for skin tumors beyond existing chemotherapeutic, immunotherapeutic, photodynamic, radiation, and surgical options are needed.

DNAzymes (*4*) have emerged as a promising new class of therapeutic agents (*5*). These single-stranded, all-DNA, catalytic molecules bind their target RNA via Watson-Crick base-pairing. DNAzymes of the "10-23" subtype cleave RNA at a predetermined junction through a de-esterification reaction (*5*–*7*). Dz13 (*8*) is a DNAzyme with 9 + 9–nucleotide RNA binding hybridization arms that cleaves the mRNA of c-*jun*, a prototypic member of the AP-1 (activating protein 1) transcription factor involved in cellular proliferation, transformation, and cell death (*9*). Dz13 has native interbase phosphodiester linkages and a 3′-3′–linked inverted T for stability. DNAzymes such as Dz13 have advantages over RNA molecules such as RNA interference or ribozymes, which are more expensive to synthesize and are subject to ribonuclease degradation. Double-stranded RNA can also initiate an interferon (IFN) response (*10*), and certain ribozymes are inefficient under physiologic conditions (*11*).

In recent years, numerous studies have provided proof-of-principle evidence that DNAzymes with different mRNA targets may serve as interventional agents in a variety of disease settings, including myocardial infarction, restenosis, glomerulonephritis, tumor growth, and spinal regeneration (*4*). However, before DNAzymes are successfully translated to the clinic as a new class of nucleic acid therapeutic, questions regarding dose-dependent effects using a therapeutic regime, sustained inhibition after cessation of therapy, and more generally, safety and biodistribution of a clinically ready DNAzyme formulation must be addressed. Here, we demonstrate that DNAzymes administered in a clinically ready liposomal formulation were safe and well tolerated in mice, rats, minipigs, and monkeys, inhibited the growth of two major skin tumor types, and enhanced antitumor immunity.

RESULTS

c-Jun DNAzyme blocks dermal SCC growth and angiogenesis

We developed dermal models of SCC and BCC in mice with lesions resembling the corresponding human skin cancer type. For SCC, immunocompromised severe combined immunodeficient (SCID) mice were injected intradermally with a suspension of T79 SCC cells

[1]Centre for Vascular Research, University of New South Wales, Sydney, New South Wales 2052, Australia. [2]Centre for Vascular Research, University of Sydney, Sydney, New South Wales 2006, Australia. [3]Centre for Vascular Research, John Curtin School of Medical Research, Canberra, Australian Capital Territory 2601, Australia. [4]Cancer and Haematology Division, Walter and Eliza Hall Institute of Medical Research, Parkville, Victoria 3052, Australia. [5]Departments of Dermatology and Biochemistry and Molecular Biology, National Cheng-Kung University Medical College and Hospital, Tainan 704, Taiwan. [6]DF Pre-Clinical Services Pty Ltd., Canberra, Australian Capital Territory 2605, Australia. [7]Dermatology Research Laboratories, University of Sydney, Sydney, New South Wales 2006, Australia.
*Present address: Department of Biological Sciences, University of Lethbridge, Lethbridge, Alberta T1K 3M4, Canada.
†Present address: Australian Regenerative Medicine Institute, Monash University, Clayton, Victoria 3800, Australia.
‡Present address: Dermatology Department, Mater Misericordiae University Hospital, Dublin 7, Ireland.
§To whom correspondence should be addressed. E-mail: L.Khachigian@unsw.edu.au

(*12*, *13*), resulting in pink/red dermal tumors (Fig. 1A). Untreated solid SCC grew exponentially in this model 15 to 20 days after dermal implantation (Fig. 1B). In this model, Dz13 [given intratumorally twice weekly in a formulation containing 1,2-dioleoyl-3-trimethylammonium-propane (DOTAP)/1,2-dioleoyl-*sn*-glycero-3-phosphoethanolamine (DOPE)] inhibited SCC growth at doses of 20 and 40 μg per injection (Fig. 1B). In contrast, Dz13scr, which has the same length and nucleotide composition as Dz13 but with scrambled hybridization arms, had no inhibitory effect at the same dose and frequency of delivery (Fig. 1B). Western blotting of whole tumor extracts (Fig. 1C) and immunohistochemical analysis of tumor cross sections (Fig. 1D) confirmed that Dz13 suppressed c-Jun. Dz13 also inhibited staining of CD31, which is

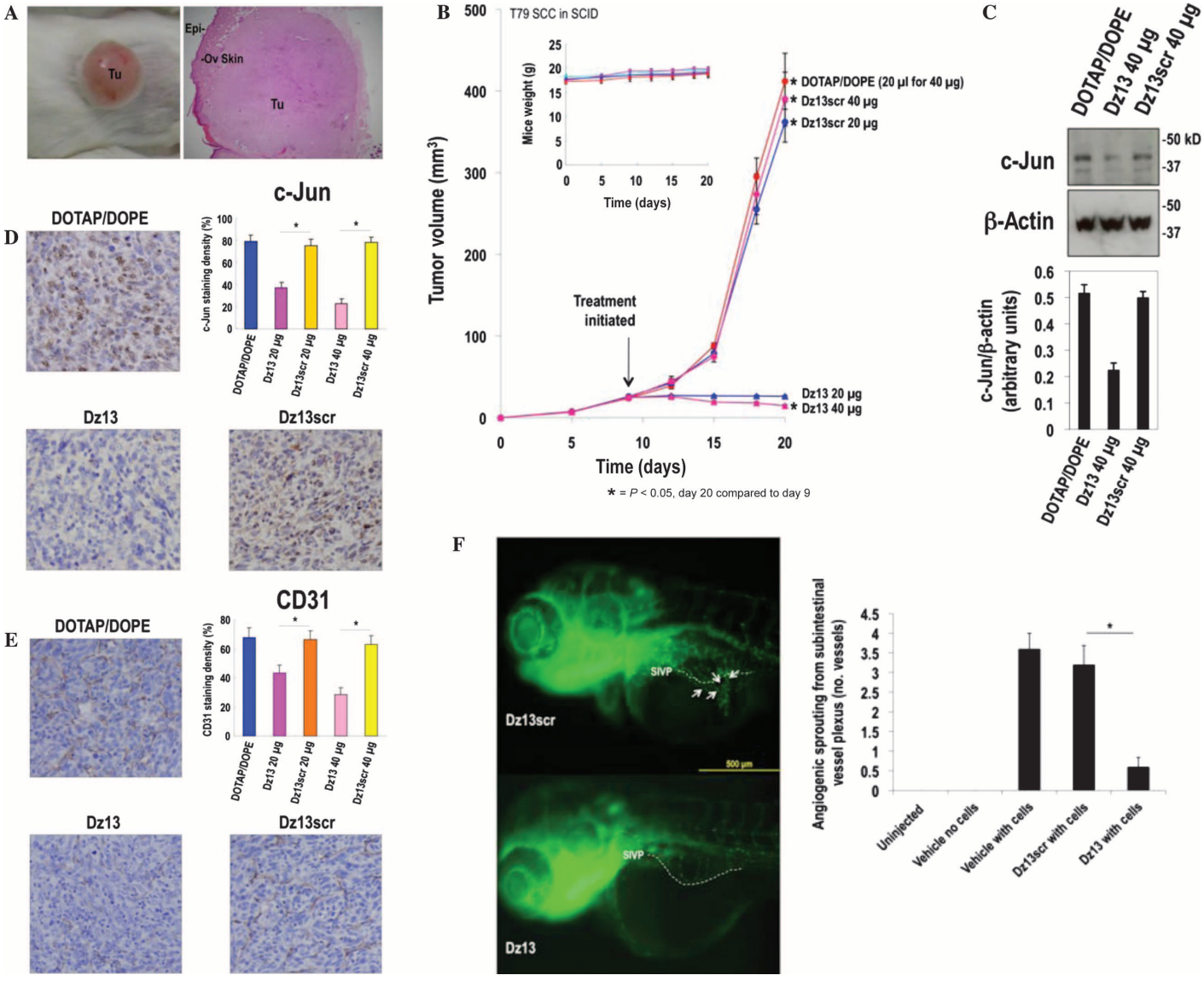

Fig. 1. Dz13 suppresses c-Jun and blocks tumor angiogenesis and dermal SCC growth. (**A**) SCID mouse bearing a typical dermal T79 SCC tumor allograft. A low-power H&E-stained cross section of tumor is also shown. Epi, epidermis; Tu, tumor; Ov, skin overlying tumor. (**B**) Dz13 inhibits T79 SCC growth in SCID mice with no effect on body weight. Treatment (Dz13, 20 or 40 μg, twice weekly, intratumoral injection) was commenced 9 days after tumor cell implantation. Data (shown here and elsewhere as means ± SEM) were analyzed by paired Student's *t* test. (**C**) Dz13 inhibits tumor c-Jun. Western blotting was performed on resected tumors (40-μg dose) at day 20 and bands were quantified by densitometry. The c-Jun and actin blots were from different gels that used identical samples because of similar molecular weights. (**D**) Immunohistochemical analysis was performed for c-Jun on resected tumors (20 or 40 μg of Dz13 or Dz13scr or vehicle) at day 20. Data were analyzed by unpaired Student's *t* test. Representative images from 40-μg group are shown. (**E**) Immunohistochemical analysis was performed for $CD31^+$ cells on resected tumors as per (D). (**F**) T79 SCC cells transfected with Dz13 or Dz13scr (0.4 μM) were injected into the perivitelline space of fli1a:EGFP transgenic zebrafish. Angiogenic sprouts from the subintestinal vessel plexus (SIVP) into the perivitelline space (arrows) were quantified under fluorescence microscopy after 48 hours. Data were analyzed by unpaired Student's *t* test.

commonly expressed on blood vessels (Fig. 1E). Using a recently described zebrafish (*Danio rerio*) model (*14*) in which tumor cells are introduced into the perivitelline space of zebrafish embryos triggering angiogenesis, we therefore explored the effect of Dz13 on the resultant neovascular response. Microinjection of a suspension of Dz13-transfected SCC cells into Fli-1/GFP (green fluorescent protein) transgenic zebrafish inhibited angiogenic sprouting within 48 hours (Fig. 1F).

Dz13 inhibition of SCC and BCC tumor growth is dose-dependent and sustained

We next determined the effect of stopping the treatment regime on tumor growth. Cessation of therapy resulted in SCC regrowth in 10 and 20 μg of Dz13-treated mice within 10 days at day 45 (Fig. 2A). In contrast, tumor regrowth was not apparent by this time in 100 μg of Dz13- treated mice (Fig. 2A). Dz13 also suppressed BCC growth after dermal implantation of BCC-1/KMC cells (*15*), and in SCID mice, Dz13 prevented the establishment of a xenograft derived from a patient with poorly differentiated facial BCC (*15*). BCC growth suppression by Dz13 was sustained to day 60, 3 weeks after the cessation of treatment (Fig. 2B).

We also examined the effects of Dz13 in a model of skin cancer metastasis. Dz13 inhibited SCC lung metastasis in mice 28 days after intravenous administration of Dz13-transfected tumor cells, whereas metastasis in the Dz13scr group did not differ from untransfected SCC (Fig. 2C).

Dz13 inhibition of SCC tumor growth involves acquired cell-mediated immunity

To examine the effect of Dz13 on SCC growth in immunocompetent mice, we used UV13-1 SCC cells (*16*, *17*) as dermal tumors in syngeneic C3H/HeN mice. Dz13 inhibited UV13-1 SCC growth in a dose-dependent manner (Fig. 3A). In this model, tumor size decreased exponentially with time, with the gradient of decay in C3H/HeN mice more than double that in SCID mice (mean, 0.14 versus 0.036 per day). These data suggested a role for the adaptive immune system in DNAzyme suppression of tumor growth. Indeed, Dz13 increased the percentage of $CD8^+$ and $CD4^+$ cells in tumors of C3H/HeN mice by three- to fourfold at 100 μg compared to Dz13scr (Fig. 3B). Moreover, $CD11b/c^+$ staining density increased twofold in Dz13-treated tumors compared to the Dz13scr group (Fig. 3B).

To further explore the contribution of the immune system in DNAzyme-mediated tumor inhibition and determine whether this effect requires the catalytic function of Dz13, we performed immunodepletion analysis in tumor-bearing C3H/HeN mice treated with Dz13 or Dz13.G>C. Dz13.G>C carries a G>C point mutation at position 6 (*18*) in the catalytic domain of the 10-23 DNAzyme (Fig. 3C). RNA cleavage experiments with a synthetic 40-nucleotide RNA

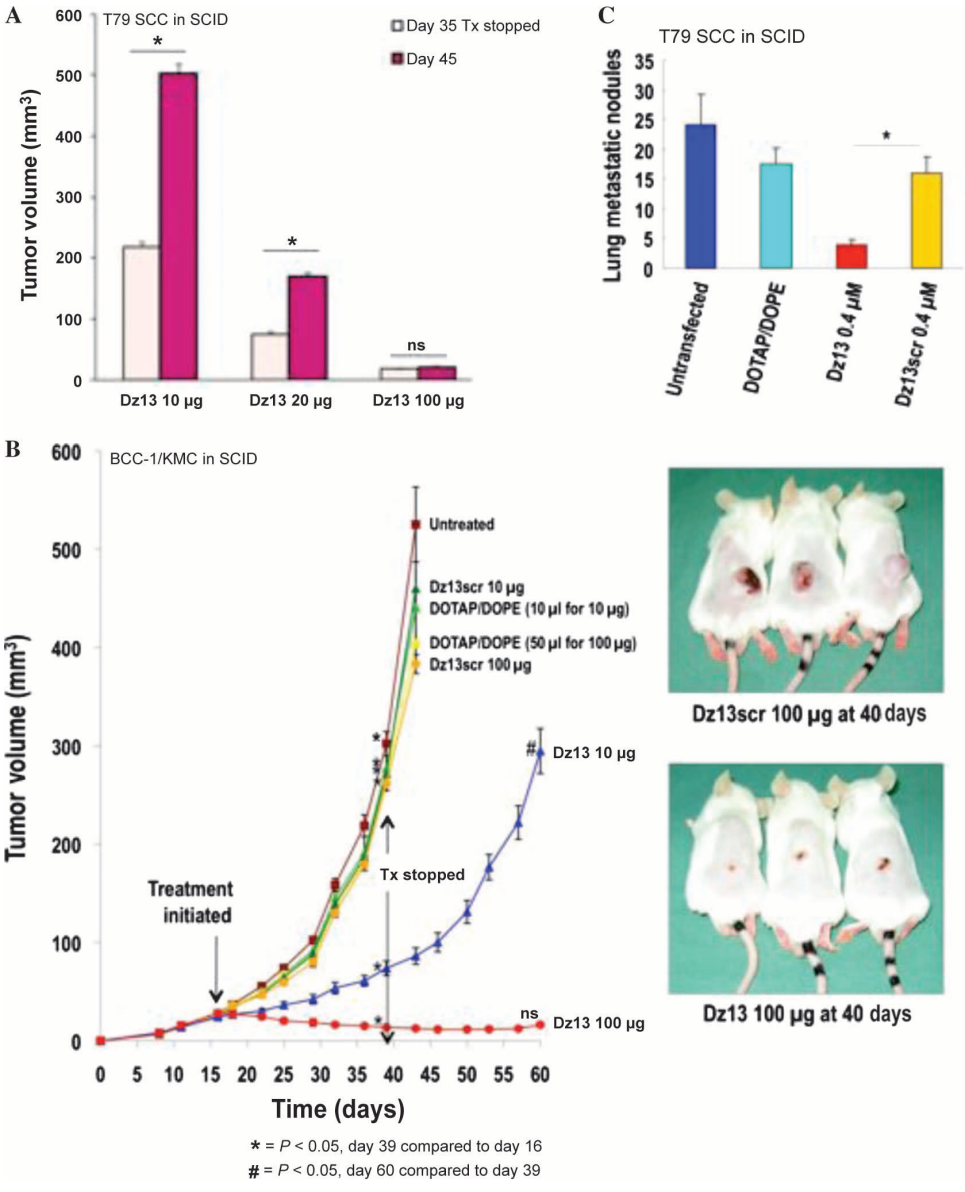

Fig. 2. Dz13 inhibition of tumor growth is dose-dependent and sustained. (**A**) T79 SCC tumors in SCID mice were treated (Tx) with 10, 20, or 100 μg of Dz13 twice weekly (starting day 11), and treatment was stopped on day 35. Tumor size is compared to day 45. Data were analyzed by paired Student's *t* test. (**B**) SCID mice bearing dermal BCC-1/KMC tumors were treated with Dz13 (10 or 100 μg, intratumorally, twice weekly) starting day 16. Treatment (Tx) was stopped on day 39 and left for another 3 weeks. Representative Dz13- and Dz13scr-treated BCC tumors in SCID mice on day 40 are shown. Data were analyzed by paired Student's *t* test. ns, not significant. (**C**) Dz13 inhibits T79 SCC metastasis to the lung. T79 SCC spread to the lung was assessed 28 days after intravenous administration of 0.4 μM Dz13- or Dz13scr-transfected tumor cells. Data were analyzed by unpaired Student's *t* test.

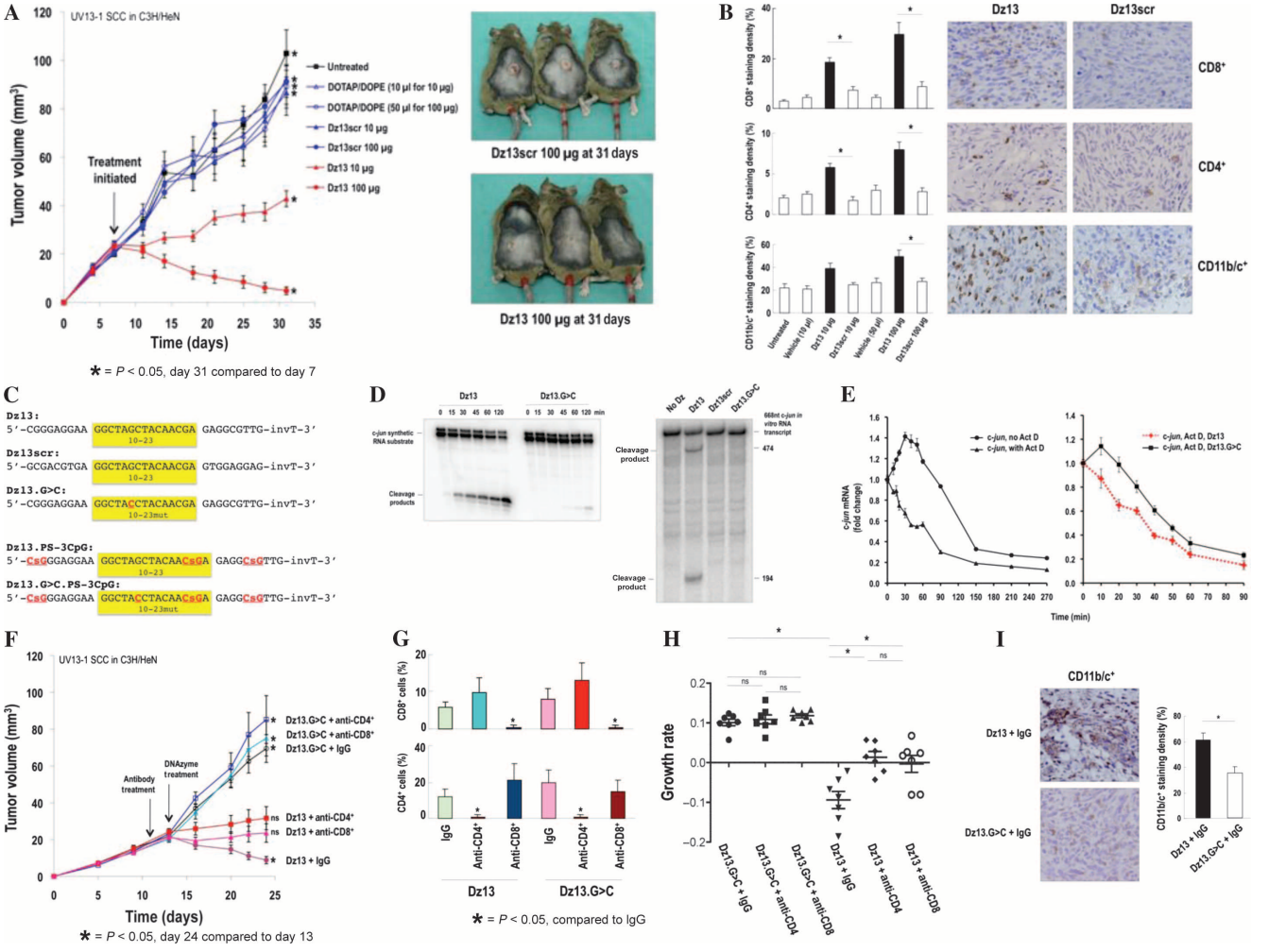

Fig. 3. Dz13 inhibition of SCC growth in immunocompetent mice involves acquired cell-mediated immunity. (**A**) Dz13 inhibits UV13-1 SCC growth in immunocompetent, syngeneic (C3H/HeN) mice. Dz13 treatment (10 or 100 μg, twice weekly, intratumorally) commenced 7 days after tumor cell implantation. Representative Dz13- and Dz13scr-treated SCC tumors in C3H/HeN mice on day 31 are shown. Data were analyzed by paired Student's *t* test. (**B**) Immunohistochemical staining was performed for $CD8^+$, $CD4^+$, and $CD11b/c^+$ cells in day 31 Dz13- and Dz13scr-treated SCC tumors in C3H/HeN mice. Representative 100 μg–treated tumors are shown. Data were derived from four mice in each group, with three fields of view from each tumor per mouse. Data were analyzed by Mann-Whitney test. (**C**) Sequences are shown for Dz13, Dz13scr, Dz13.G>C, Dz13.PS-3CpG, and Dz13.G>C.PS-3CpG. The 10-23 domain is boxed. Mut, mutation in the catalytic domain. The CsG modification (where "s" represents a phosphorothioate, rather than a phosphodiester linkage) is indicated. (**D**) Dz13 cleavage of a 40-nucleotide synthetic RNA substrate after various times at 37°C or an in vitro–transcribed 668-nucleotide murine c-*jun* mRNA after 2 hours at 37°C, each containing the Dz13 cleavage site, but not with Dz13.G>C nor Dz13scr. The larger upper band using the 40-nucleotide substrate likely represents secondary structure. (**E**) Dz13 increases endogenous c-*jun* mRNA instability. Real-time PCR measuring c-*jun* mRNA of growth-quiescent T79 SCC cells that had been incubated with medium containing serum for 30 min before exposure to actinomycin D (Act D, 10 μg/ml) and incubated for the times indicated. Alternatively, the cells were transfected overnight with 0.4 μM Dz13 or Dz13.G>C and then serum-induced for 30 min and incubated with actinomycin D for the times indicated before harvest. Data were expressed as fold change relative to the serum-starved control treated with fetal bovine serum (FBS) for 30 min (no actinomycin D). Data represent compilation of four experiments. (**F**) Alleviation, by immunodepletion, of Dz13-suppressed UV13-1 SCC tumor growth in syngeneic (C3H/HeN) mice. Antibodies were injected (100 μg, intraperitoneally) on days 11 and 13 and then weekly into tumor-bearing mice treated with DNAzyme (100 μg, twice weekly, intratumorally, commencing day 13). Data were analyzed by paired Student's *t* test. (**G**) Flow cytometric assessment of blood $CD8^+/CD4^+$ populations in mice at day 24 injected with control IgG, anti-CD4, or anti-CD8 IgG antibodies. Data were analyzed by Mann-Whitney test. (**H**) Comparison of tumor growth rates for each C3H/HeN mouse ($n = 7$ per group) treated with DNAzyme (relative to day 13). A mean decay rate of Dz13-treated tumors was 0.094 per day (tumor size decreased with half-life of 7.4 days; hereafter, mean decay/growth rates are described in terms of half-lives/doubling times for convenience), whereas Dz13.G>C-treated tumors grew with a doubling time of 6.9 days. The rates of growth/decay between Dz13.G>C + IgG and Dz13 + IgG were significantly different ($P = 0.0006$). There was no difference in tumor growth between control IgG and T cell–depleted groups in Dz13.G>C-treated mice ($P = 0.25$, Kruskal-Wallis). Tumor growth rates were higher in Dz13-treated mice after either $CD4^+$ cell depletion (doubling time, 51 days) or $CD8^+$ cell depletion (half-life of decay, 227 days) than in IgG-treated controls [half-life of decay = 7.4 days ($P < 0.05$, Kruskal-Wallis with Dunn's multiple-comparison test)], but growth rate of $CD4^+$ cell–depleted tumors did not differ from $CD8^+$ cell–depleted tumors ($P > 0.05$). (**I**) $CD11b/c^+$ cells in Dz13- and Dz13.G>C-treated SCC tumors in C3H/HeN mice. Data were derived from four mice in each group, with three fields of view from each tumor per mouse. Data were analyzed by Mann-Whitney test.

substrate or considerably longer in vitro–transcribed 668-nucleotide RNA substrate confirmed that the G_6>C_6 point mutation ablates the catalytic activity of Dz13 (Fig. 3D). Indeed, in T79 SCC cells treated with actinomycin D to block new c-*jun* mRNA expression (Fig. 3E, left), the stability of c-*jun* transcript was decreased with Dz13 when compared with the catalytic mutant Dz13.G>C (Fig. 3E, right).

Thus, we compared the effect of Dz13 and Dz13.G>C (100 μg, intratumorally, twice weekly) on tumor size in mice injected with rat anti-mouse CD4 immunoglobulin G (IgG) (GK1.5, 100 μg, intraperitoneally, weekly), rat anti-mouse CD8 IgG (53.6.7, 100 μg, intraperitoneally, weekly), or control rat IgG (Mac-4, 100 μg, intraperitoneally, weekly) (*19*). Tumor growth in C3H/HeN mice was inhibited by Dz13 compared with the catalytically mutated Dz13.G>C, indicating that the catalytic domain of Dz13 contributes to this antitumor effect (Fig. 3F).

Comparison of tumor growth in the Dz13 + anti-CD4 or Dz13 + anti-CD8 groups with that of the Dz13 + IgG group revealed that tumor inhibition affected by Dz13 was significantly reduced in mice lacking either $CD4^+$ or $CD8^+$ cells (Fig. 3F). Flow cytometry confirmed that target T cell immunodepletion was successfully achieved using this strategy: Anti-CD4 and anti-CD8 antibodies depleted circulating $CD4^+$ and $CD8^+$ cells, respectively, in tumor-bearing mice (Fig. 3G). Tumor growth rate in $CD4^+$-depleted mice did not differ from $CD8^+$-depleted mice. Immunodepletion resulted in growth inhibition rather than decay; this effect was again dependent on catalytically active Dz13 (Fig. 3H). In addition, consistent with Dz13scr-treated tumors (Fig. 3B, lower), we noted fewer $CD11b/c^+$ cells in Dz13.G>C-treated tumors than in Dz13-treated tumors (Fig. 3I). These data suggest that adaptive immune mechanisms are involved in Dz13 tumor inhibition and that this response requires the catalytic domain of the DNAzyme.

Dz13 inhibits mitogenesis and increases apoptosis in the SCC tumors

Dz13 inhibited expression of the mitogenic markers PCNA (proliferating cell nuclear antigen) and CDK4 (cyclin-dependent kinase 4) and increased expression of the CDK inhibitor $p21^{WAF1/Cip1}$ in SCC tumors (Fig. 4A). It also inhibited the tumorigenic markers matrix metalloproteinases 2 and 9 (MMP-2 and MMP-9), vascular endothelial growth factor A (VEGF-A), and fibroblast growth factor 2 (FGF-2) (Fig. 4B), which suggests that mitogenesis is a target of Dz13 in SCC. In addition, Dz13 (0.4 μM with DOTAP/DOPE) increased apoptosis

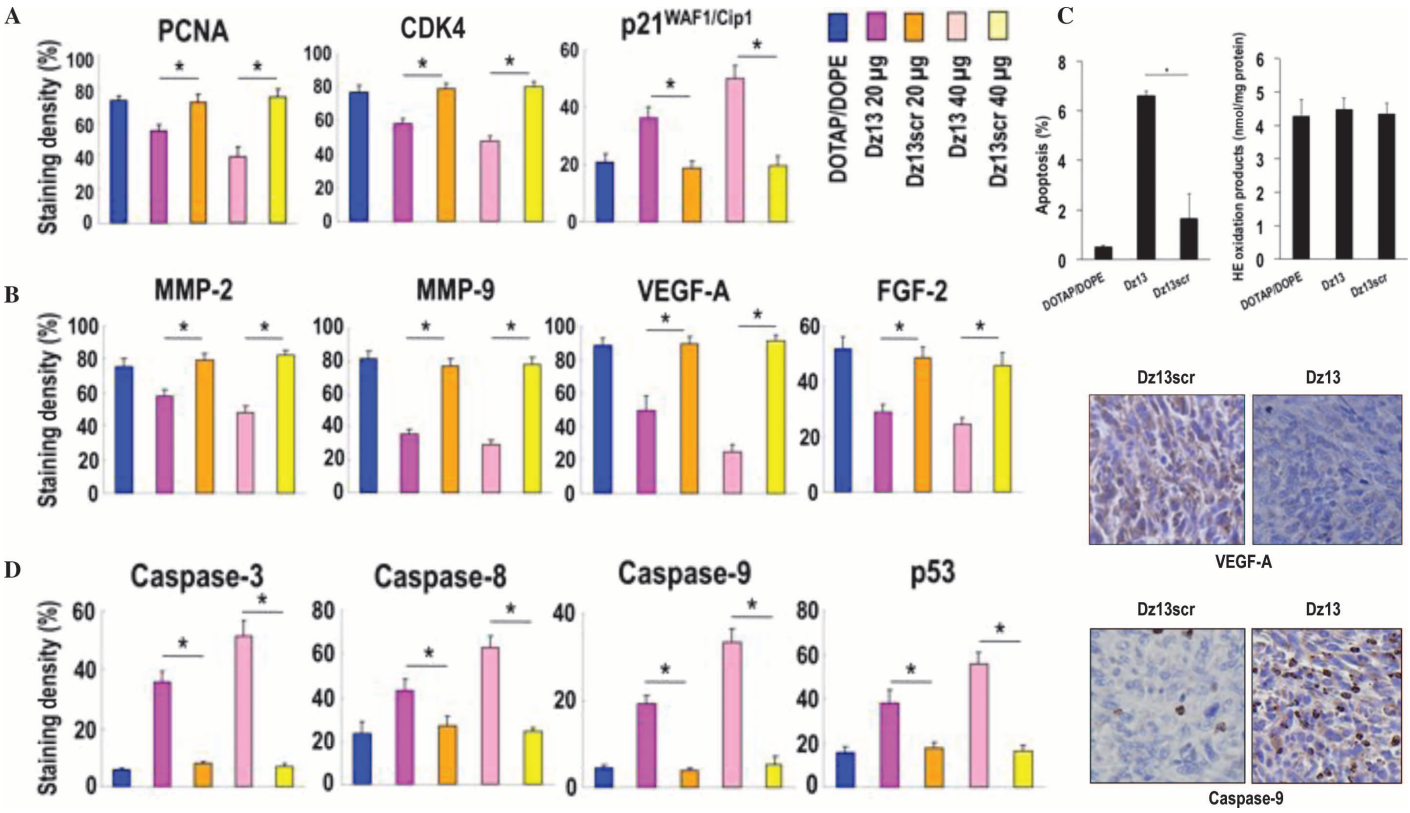

Fig. 4. Dz13 suppresses mitogenesis and increases apoptosis in the tumors. (**A** and **B**) Immunohistochemical staining was performed for (A) PCNA, CDK4, and $p21^{WAF1/Cip1}$ or (B) MMP-2, MMP-9, VEGF-A, and FGF-2 in T79 SCC tumors resected from Dz13- and Dz13scr-treated (20 and 40 μg, intratumorally, twice weekly) SCID mice on day 20. Data were analyzed by unpaired Student's *t* test. (**C**) Dz13 stimulates annexin V^+ staining. T79 SCC cells were transfected with 0.4 μM Dz13 or Dz13scr, and after 24 hours, apoptosis was determined by annexin V staining and flow cytometry. Data were analyzed by unpaired Student's *t* test. Oxidative stress was determined using an LC-MS/MS assay for hydroethidine and its oxidation products. Three separate experiments were performed, each in triplicate. Data were analyzed by the Mann-Whitney rank-sum test. (**D**) Dz13 stimulates caspase-3, caspase-8, caspase-9, and p53 in the tumors. Immunohistochemical staining was performed for caspase-3, caspase-8, caspase-9, and p53 in T79 SCC tumors resected from Dz13-treated SCID mice on day 20. Data were analyzed by unpaired Student's *t* test. Representative staining is shown for VEGF-A and caspase-9 (40-μg dose).

at least fivefold as determined by annexin V staining in T79 SCC cells (Fig. 4C). However, oxidative stress in these cells was not induced by Dz13 relative to Dz13scr or the vehicle control, as determined by liquid chromatography–tandem mass spectrometry (LC-MS/MS) analysis of hydroethidine and its oxidation products [2-hydroxy-ethidium ($2OHE^+$) and ethidium (E^+)] (Fig. 4C). Instead, Dz13 increased expression of the proapoptotic markers caspase-3, caspase-8, caspase-9, and p53 (Fig. 4D).

Dz13 inhibits SCC tumor growth independently of CpG motifs

CpG oligonucleotides are short single-stranded synthetic DNA molecules that can serve as immunostimulants (*20*), due at least in part to recognition by Toll-like receptor 9 (TLR9) (*21*). Several lines of evidence indicate that Dz13 inhibition of skin tumor growth does not involve CpG motifs. First, Dz13.G>C, which retains the same three CpG motifs in Dz13 because the binding arms of the DNAzyme are not scrambled (Fig. 3C), affects tumor growth distinctly from Dz13 in both immunodeficient and immunocompetent mice (Figs. 5A and 3F, respectively). Second, Dz13scr, which also has three CpG motifs (Fig. 3C), does not inhibit tumor growth in immunodeficient or immunocompetent mice, unlike Dz13 (for example, Figs. 1B, 2B, 3A, and 5A). Third, we introduced phosphorothioate (PS) linkages at the three CpG motifs into Dz13 (to produce Dz13.PS-3CpG). TLR9 responsiveness triggered by CpG motifs is mainly associated with PS, rather than native phosphodiester interbase linkages in the oligonucleotide (*22*, *23*). However, Dz13.PS-3CpG did not potentiate DNAzyme inhibition of tumor growth over native Dz13 (Fig. 5A). Indeed, Dz13 caused potent inhibition of tumor growth, whereas Dz13.G>C (like Dz13scr) had no effect (Fig. 5A). We did not detect by enzyme-linked immunosorbent assay (ELISA) a significant difference in serum IFN-α or interleukin-6 (IL-6), which would be an indication of a TLR9 response (*24*), in tumor-bearing mice treated with Dz13, Dz13.G>C, or Dz13scr. However, we did detect a small change in serum IFN-α and IL-6 in mice treated with the two PS-modified DNAzymes (Dz13.PS-3CpG and Dz13.G>C.PS-3CpG) (Fig. 5B). These findings therefore suggest that the three CpGs in Dz13 are not responsible for the antitumor activity of the DNAzyme.

To demonstrate cleavage-dependent DNAzyme inhibition of tumor growth, we performed quantitative real-time polymerase chain reaction (PCR) analysis [using glyceraldehyde-3-phosphate dehydrogenase (GAPDH) as an internal loading control] to assess c-*jun* mRNA in tumors treated with Dz13 or with Dz13.G>C. This analysis revealed that Dz13 and Dz13.PS-3CpG reduced c-*jun* mRNA in the tumors, whereas neither Dz13.G>C, Dz13.G>C.PS-3CpG, nor Dz13scr influenced c-*jun* mRNA (Fig. 5C, upper). We also quantified c-Jun in the tumors (from Fig. 5A) using a Western blot approach in which we compared tumor c-Jun against a standard curve constructed with recombinant c-Jun, followed by scanning densitometric analysis. c-Jun protein levels paralleled mRNA (Fig. 5C, lower). These findings show that Dz13 inhibited c-*jun* mRNA and protein in the tumors, and that DNAzyme inhibition of c-Jun requires an intact catalytic domain.

Biodistribution, stability, and safety of Dz13

Biodistribution analysis and toxicology studies are essential for the clinical evaluation of candidate drugs. Therefore, good laboratory practice (GLP)–compliant plasma distribution studies were performed in Sprague-Dawley rats. After a single intravenous administration of ^{33}P-labeled Dz13, total plasma radioactivity steadily declined over time (Table 1). The mean plasma concentration at 24 hours was 21.9% of the load at the first sampling point of 1 hour. After single intradermal administration, 35.9% of the 1 hour after dose radioactivity was detected in the systemic circulation 24 hours after dosing (Table 2), indicating that ^{33}P-Dz13 was retained for at least 24 hours after delivery by either route. In a separate mouse study, about 5 to 10% of ^{33}P-Dz13 was retained in the tumor after intratumoral injection for at least 9 hours. Dz13 accumulated, albeit transiently, in the liver as amounts of Dz13 decreased in the tumor (Fig. 6A). Analysis

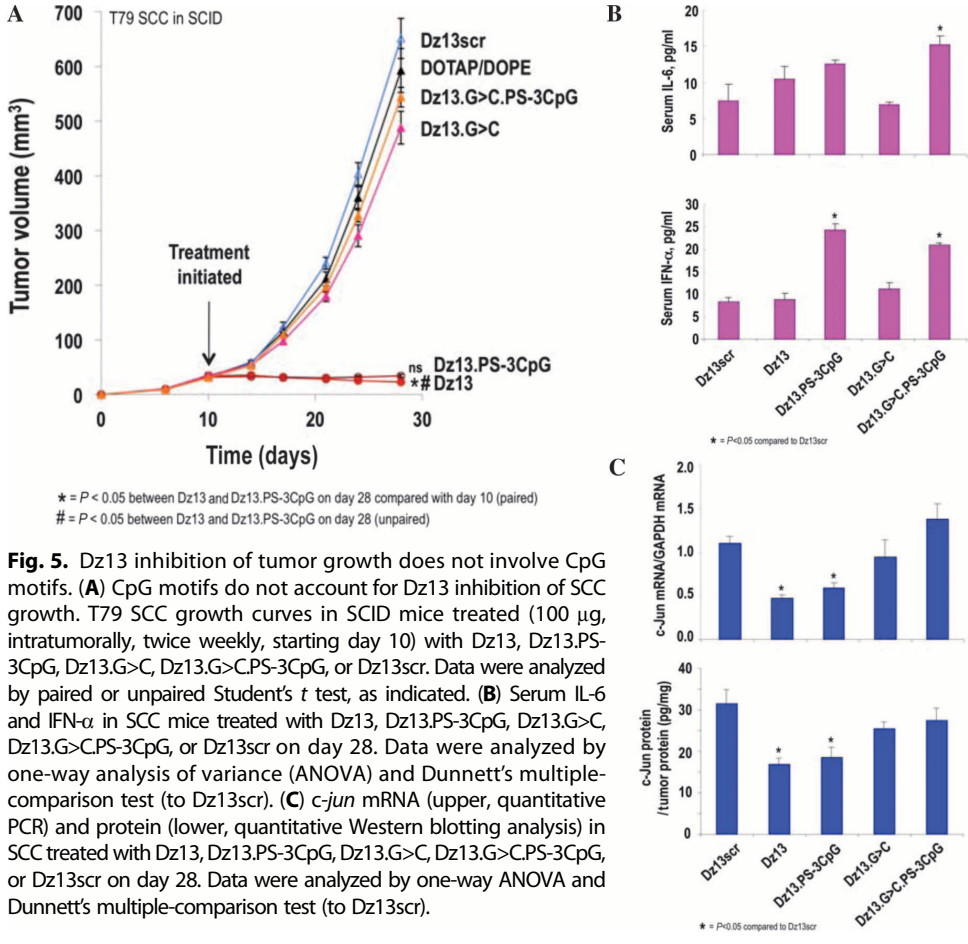

Fig. 5. Dz13 inhibition of tumor growth does not involve CpG motifs. (**A**) CpG motifs do not account for Dz13 inhibition of SCC growth. T79 SCC growth curves in SCID mice treated (100 μg, intratumorally, twice weekly, starting day 10) with Dz13, Dz13.PS-3CpG, Dz13.G>C, Dz13.G>C.PS-3CpG, or Dz13scr. Data were analyzed by paired or unpaired Student's *t* test, as indicated. (**B**) Serum IL-6 and IFN-α in SCC mice treated with Dz13, Dz13.PS-3CpG, Dz13.G>C, Dz13.G>C.PS-3CpG, or Dz13scr on day 28. Data were analyzed by one-way analysis of variance (ANOVA) and Dunnett's multiple-comparison test (to Dz13scr). (**C**) c-*jun* mRNA (upper, quantitative PCR) and protein (lower, quantitative Western blotting analysis) in SCC treated with Dz13, Dz13.PS-3CpG, Dz13.G>C, Dz13.G>C.PS-3CpG, or Dz13scr on day 28. Data were analyzed by one-way ANOVA and Dunnett's multiple-comparison test (to Dz13scr).

Table 1. Kinetics of ^{33}P-Dz13 in plasma after a single intravenous administration of ^{33}P-Dz13 to male rats. After intravenous administration of ^{33}P-labeled Dz13 into Sprague-Dawley rats (target dose level, 180 μg/kg), the mean plasma concentration of total radioactivity at 1 hour after dose (the first sample time point) was 97.4 ng equivalents/g. Results from four rats are shown and expressed as nanogram equivalents per gram.

Time point (hours)	001M	002M	003M	004M	Mean	SD
1	72.9	107.0	112.9	96.7	97.4	17.6
2	41.8	56.1	46.6	52.8	49.3	6.4
4	26.9	42.4	40.0	37.8	36.8	6.9
6	32.7	34.1	39.0	36.8	35.7	2.8
8	30.3	32.6	39.7	30.9	33.4	4.3
12	25.5	23.4	27.6	39.3	29.0	7.1
16	22.6	21.7	23.8	21.4	22.4	1.1
24	19.4	22.5	23.4	20.3	21.4	1.9

of tumor DNA extracts 1 hour after ^{33}P-Dz13 delivery revealed no degradation of DNAzyme in vivo (Fig. 6A, inset). Incubation of ^{33}P-Dz13 in serum at 37°C also showed no detachment of ^{33}P from the DNAzyme for up to 120 hours, whether in the absence or presence of DOTAP/DOPE (Fig. 6B).

Dz13 safety and tolerability with DOTAP/DOPE as carrier was demonstrated by several criteria. Dz13 did not adversely affect body weight (Fig. 1B, inset) or a diverse array of hematologic and thrombotic parameters in tumor-bearing mice treated intratumorally with DNAzyme (table S1), nor did it influence weight, food intake, or clinical biochemistry when administered intradermally or intravenously in cynomolgus monkeys, minipigs, and rats. GLP-compliant repeat-dose toxicology studies were conducted in cynomolgus monkeys administered with Dz13/DOTAP/DOPE intravenously at doses up to 180 μg/kg each day for 28 days followed by a 2-week nontreatment recovery period. No significant clinical hematology, urinalysis, clinical biochemistry, necropsy, or organ histological treatment-related changes were reported at the end of the 28-day dosing interval (Table 3) or after the 2-week recovery period. It is important to note that, because transient liver accumulation of Dz13 was reported in mice after intratumoral administration, no evidence of liver changes was observed on close examination of clinical biochemistry, necropsy, organ weight, or histology results from the repeat-dose cynomolgus monkey study. The highest dose examined (180 μg/kg per day) equates to a human equivalent dose based on body surface area of 57.6 μg/kg per day (*25*) or 34-fold of a proposed clinical intratumoral dose of 100 μg of Dz13 per 60 kg of adult. Moreover, Dz13 did not interfere with cardiac function [as assessed by electrocardiogram (ECG) in the cynomolgus monkey repeat-dose toxicology study], nor did it alter hERG potassium channel function at 200-fold the maximal plasma load of a 100-μg clinical dose (Table 4).

A further GLP-compliant repeat-dose study in rats was performed in which Dz13/DOPE/DOTAP (total Dz13 dose of 800 μg) was administered by intradermal injection. A total of eight injections (two injections per test site per day; four injection sites) were administered during the initial 4 days of the 7-day study. No hematology or clinical biochemistry abnormalities were reported. In addition, a GLP-compliant local tolerance study was completed in minipigs whose skin closely resembles that of humans, in which 100 μg of Dz13 in a 50-μl solution containing DOTAP/DOPE was injected intradermally on days 1 and 4 of a 7-day study. Dz13 was well tolerated, with no abnormal clinical signs or adverse effects on body weight and food intake, and there were no abnormal necropsy findings, although the carrier DOTAP/DOPE showed minor histological evidence of dermal irritation (Table 5). Finally, Dz13 did not interfere in more than 70 enzyme-linked and radioligand-binding assays of biologically relevant targets (at a standard upper concentration of 1 μM that equates to 500 times the maximum plasma load of a 100-μg injection) (table S2). These preclinical data suggest that Dz13 may be safe and well tolerated when administered to humans.

DISCUSSION

The incidence of skin cancer continues to increase worldwide (*26*), and alternative treatments beyond existing chemotherapeutic, immunotherapeutic, photodynamic, radiation, and surgical options are needed. Here, we show that Dz13 inhibited the growth of two common skin cancer types, BCC and SCC, in mice. DNAzyme inhibition was sequence-specific, and growth inhibition was sustained after stopping Dz13 treatment. This study demonstrates successful intratumoral therapy in an animal skin cancer model using a clinically ready DNAzyme formulation.

Dz13 blocked tumor growth in both immunodeficient and immunocompetent syngeneic mice. However, tumor decay rate was considerably greater in immunocompetent mice than in immunodeficient mice, which suggests a role for the immune system in Dz13 tumor control. In support of this, Dz13 increased the percentage of tumor-infiltrating $CD4^+/CD8^+$ populations in C3H/HeN mice when compared to Dz13scr-treated tumors, and $CD4^+$ or $CD8^+$ immunodepletion in immunocompetent mice resulted in loss of Dz13-dependent tumor

Table 2. Kinetics of ^{33}P-Dz13 in plasma after a single intradermal administration of ^{33}P-Dz13 to male rats. After intradermal administration of ^{33}P-labeled Dz13 into Sprague-Dawley rats (target dose level, 333 μg/kg), the mean plasma concentration of total radioactivity at 1 hour after dose (the first sample time point) was 56.5 ng equivalents/g. Results from four rats are shown and expressed as nanogram equivalents per gram. NS, no sample.

Time point (hours)	005M	006M	007M	008M	Mean	SD
1	65.9	78.9	58.7	22.5	56.5	24.2
2	48.6	65.6	49.9	18.6	45.7	19.6
4	50.7	65.8	41.8	18.2	44.1	19.9
6	NS	70.3	44.4	19.3	44.7	25.5
8	48.1	63.0	37.6	15.7	41.1	19.9
12	29.5	35.5	23.2	12.6	25.2	9.8
16	21.9	35.9	24.1	11.7	23.4	9.9
24	19.4	30.8	19.8	11.2	20.3	8.0

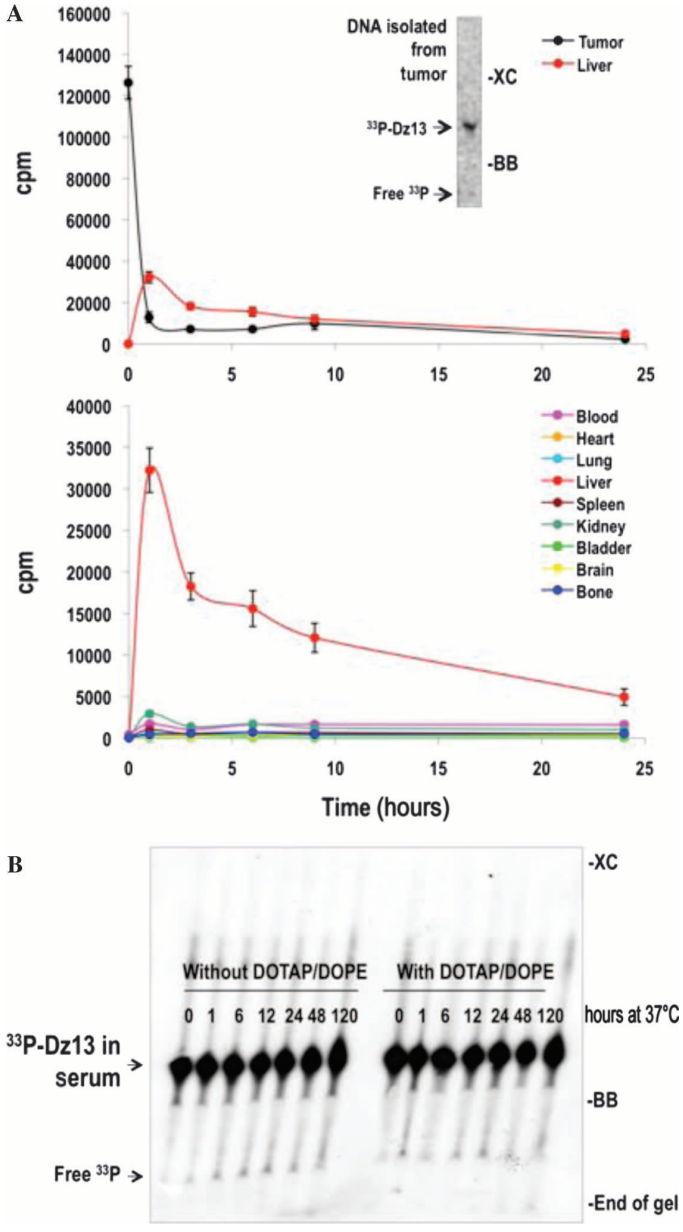

Fig. 6. Biodistribution, stability, and safety of administered Dz13 to animals. (**A**) Biodistribution of ^{33}P-Dz13 in T79 SCC tumor-bearing mice. Dz13 (40 μg of Dz13 spiked with ^{33}P-Dz13) was injected intratumorally into T79 SCC tumor-bearing SCID mice, and after various times, the mice were killed; tumors, organs, and blood were collected; and radioactivity was assessed. Inset, ^{33}P-Dz13 resected from the tumor 1 hour after intratumoral delivery remained intact after resolution by 6% denaturing PAGE followed by autoradiography. XC, xylene cyanol; BB, bromophenol blue. (**B**) Stability of ^{33}P-Dz13 in FBS at 37°C. ^{33}P-Dz13 was incubated in DMEM containing 40% FBS at 37°C, and at various times, denaturing loading buffer was added and the samples were loaded on a 6% denaturing PAGE gel before autoradiography.

decay. CD8$^+$ T cells underpin adoptive immunotherapy strategies for cancer (*27*, *28*) and may contribute to dendritic cell activation–mediated antitumor activity of some chemotherapies and irradiation (*29*, *30*).

Table 3. Dz13/DOTAP/DOPE 28-day repeat intravenous dose toxicology GLP study in cynomolgus monkeys. Monkeys were administered with Dz13/DOTAP/DOPE intravenously at doses up to 180 μg/kg per day for 28 days followed by a 2-week nontreatment recovery period. NSTRE, no significant treatment-related effect.

	Dz13 (μg/kg per day)		
	20	60	180
Clinical signs	NSTRE	NSTRE	NSTRE
Body weight	NSTRE	NSTRE	NSTRE
Food and water intake	NSTRE	NSTRE	NSTRE
Ophthalmology	NSTRE	NSTRE	NSTRE
Electrocardiogram	NSTRE	NSTRE	NSTRE
Clinical biochemistry	NSTRE	NSTRE	NSTRE
Bone marrow analysis	NSTRE	NSTRE	NSTRE
Urinalysis	NSTRE	NSTRE	NSTRE
Organ weight	NSTRE	NSTRE	NSTRE
Histopathology	NSTRE	NSTRE	NSTRE

CD4$^+$ T cells have also been implicated in mediating regression of human skin cancers (*31*). Recent studies have shown that CD4$^+$ T cells regulate angiogenesis in the tumor microenvironment and contribute to tumor regression upon oncogene inactivation (*32*). Here, we implicate a previously unrecognized phenomenon of immune system involvement during tumor suppression by a DNAzyme that depends on both CD4$^+$ and CD8$^+$ T cells. Thus, Dz13 may inhibit tumor growth by at least two mechanisms: directly, by suppression of c-Jun and c-Jun–dependent proangiogenic and tumorigenic genes (such as VEGF-A, FGF-2, MMP-2, and MMP-9), and indirectly, by an immune-mediated mechanism, perhaps exposing tumor antigens for recognition and attack by the immune system (*33*).

A point mutation that ablates the catalytic activity of Dz13 (G_6>C_6) abrogates Dz13 tumor inhibition in both immunodeficient and immunocompetent mice. Moreover, the three native CpGs in Dz13 are not responsible for the antitumor activity of the DNAzyme, suggesting that activation of innate immunity through TLR9 is not involved. However, a role for innate immune mechanisms cannot be excluded. We found fewer CD11b/c$^+$ cells in Dz13.G>C-treated tumors than in Dz13-treated tumors (Fig. 3I), consistent with fewer CD11b/c$^+$ cells in Dz13scr-treated tumors relative to Dz13 tumors (Fig. 3B, lower). These data suggest that inflammation in growth-suppressed tumors caused by Dz13 may relate to its catalytic domain.

Intratumoral oligonucleotide delivery has certain advantages over systemic administration. Local administration offers precise drug delivery, higher local drug concentrations than can be achieved by systemic chemotherapy, and the reduced propensity of systemic toxic side effects. Local delivery may also provide greater efficacy. For example, intratumorally administered CpG oligonucleotide improved the efficacy of rituximab against established tumors, whereas systemically administered CpG did not achieve tumor eradication either with or without rituximab (*34*). Although a topical route of delivery may be more clinically appealing than intratumoral injection, the DNAzyme may not sufficiently penetrate the lesion or skin unless aided by electroporation

Table 4. Relative hERG tail current inhibition. The whole-cell patch-clamp technique was used to investigate the effects of the agents indicated on hERG potassium channels stably expressed in HEK 293 cells.

Test agent and concentration	Relative tail current (%)	Mean (%) ± SE
Vehicle (negative control A0049)*	102.45	99.97 ± 1.82
	101.05	
	96.41	
Dz13 (0.4 ng/μl) in DOTAP/DOPE (0.3 ng/μl)	96.77	98.64 ± 1.68
	97.16	
	102.0	
Dz13 (1.33 ng/μl) in DOTAP/DOPE (1 ng/μl)	96.05	98.61 ± 2.21
	103.01	
	96.76	
Dz13 (4.0 ng/μl) in DOTAP/DOPE (3 ng/μl)	101.01	96.92 ± 2.17
	96.15	
	93.62	
Dz13 (13.33 ng/μl) in DOTAP/DOPE (10 ng/μl)	92.94	92.13 ± 0.43
	91.99	
	91.46	
100 nM E-4031 (positive control)†	11.20	8.46 ± 2.11
	9.86	
	4.31	

*The vehicle (A0049) was prepared by mixing water for injection (WFI) and ethanol [1.67:1 (v/v)]. To this mix, DMEM was added in a ratio of 2:3 (v/v) (WFI/ethanol/DMEM). †Selective I_{Kr} blocker (E-4031).

Table 5. Dz13/DOTAP/DOPE local tolerance test in minipigs. Male Göttingen ApS minipigs received Dz13 at a dose of 100 μg in combination with or without DOTAP/DOPE in DMEM as a 50-μl injection on two occasions (days 1 and 4). The three animals each received DMEM, Dz13/DOTAP/DOPE (in DMEM), Dz13 (in DMEM), and DOTAP/DOPE (in DMEM) into four marked injection sites (one site per formulation) on the back of each animal, resulting in eight total injections into four sites (two injections per site). The study was terminated on day 7.

	Dz13 (100 μg)/DOTAP/DOPE (in DMEM)
Clinical signs	NSTRE
Body weight	NSTRE
Food intake	NSTRE
Necroscopy*	NSTRE
Histopathology	Minor irritant reaction in dermis†,‡

*Detailed examination of the external features and internal orifices (ears, nostrils, mouth, anus, and vulva) and cranial, thoracic, abdominal organs, injection sites, and tissues. †Serocellular crust was present in the keratin layer of the epidermis in one animal at injection site 1 (DMEM) and two animals at injection site 2 (Dz13/DOTAP/DOPE in DMEM). This was considered to be due to the injection procedure. ‡Minimal to mild deposition of test material was present at injection site 2 (Dz13/DOTAP/DOPE in DMEM) in two animals, and in two animals at injection site 4 (DOTAP/DOPE in DMEM). There was an accompanying inflammatory cell reaction. This minor irritant reaction was considered to be due to the administration of vehicle (DOTAP/DOPE in DMEM) and not a toxicological effect of administration of Dz13.

(*35*). Indeed, the pharmacokinetics of intratumoral Dz13 administration are favorable for clinical use. After single intratumoral administration, about 5 to 10% of ^{33}P-Dz13 was retained in the tumor for at least 9 hours, and after single intravenous and intradermal administration of ^{33}P-Dz13 in GLP-compliant plasma distribution studies, the mean plasma ^{33}P-Dz13 concentration at 24 hours was 21.9 and 35.9% (respectively) of total radioactivity recorded 1 hour after dose. Current limitations in the in vivo use of DNAzymes include the requirement of a transfection agent to facilitate optimal cellular delivery and, accordingly, practical considerations such as formulation before injection and limitations of DNAzyme use in a systemic setting rather than the local route used here.

Dz13, in a clinically ready formulation, is safe in a series of GLP-compliant toxicology studies and effective in a range of preclinical skin cancer models. No toxicity was evident in a GLP-compliant nonhuman primate toxicology study (as assessed by classical means), even at 34 times the maximum proposed intratumoral clinical dose of 100 μg of Dz13. Here, no alteration in ECG was reported at the maximum dose (180 μg/kg intravenously). In vitro hERG channel function was not affected at concentrations 200 times that expected in the plasma at the maximum proposed intratumoral clinical dose (100 μg). Similarly, no Dz13 toxicity was found in a GLP-compliant repeat-dose local tolerance study in minipigs. Finally, there was no nonspecific Dz13 activity observed in more than 70 separate biologically relevant assays at 500 times the maximal plasma load achieved with the 100-μg dose. These studies demonstrate the suitability of DNAzymes as drug candidates for evaluation in a "first-in-human" clinical trial.

MATERIALS AND METHODS

Cell culture

T79 and UV13-1 SCC were cultured in Dulbecco's modified Eagle's medium (DMEM) (Invitrogen). Human BCC-1/KMC cells (*2*) were cultured in RPMI 1640 complete medium (Invitrogen). Cells were passaged as previously described (*36*, *37*).

DNAzymes and carriers

DNAzymes with 3′-3′–linked inverted T were produced and high-performance liquid chromatography–purified by TriLink Biotechnology. DOTAP and DOPE were obtained in powder form from Avanti Polar Lipids.

In vitro transcription and cleavage experiments

^{32}P-labeled 668-nucleotide murine c-*jun* RNA transcript was prepared by in vitro transcription of pBluescript containing the insert with the MEGAscript kit (Ambion). The cleavage reaction was performed at 37°C for 2 hours in 10 mM $MgCl_2$, 5 mM tris (pH 7.5), 150 mM NaCl, 0.9 pmol RNA substrate, and 45 pmol DNAzyme. Samples and ^{32}P-labeled RNA Century Plus Markers (Ambion) were run on 6% denaturing polyacrylamide-urea gels. Alternatively, synthetic c-*jun* RNA substrate (40 nucleotides) spanning the Dz13 cleavage site, 5′-UGCCCUCAACGCCUCGUUCCUCCCGUCCGAGAGCGGACCU-3′, was ^{32}P-labeled with T4 polynucleotide kinase and purified with NucAway spin columns (Ambion). Reactions were performed at 37°C for 0, 15, 30, 45, 60, and 120 min in 10 mM $MgCl_2$, 5 mM tris (pH 7.5), 150 mM NaCl with 100 nM labeled substrate, and 10 nM DNAzyme.

Samples were run on 12% denaturing polyacrylamide-urea gels, and signal was visualized by autoradiography with an FLA-7000 Fujifilm phosphorimager.

Real-time PCR for c-*jun* mRNA stability studies in T79 SCC cells

Total RNA from T79 SCC untransfected or transfected with 0.4 μM Dz13 or Dz13.G>C was extracted after the cells were serum-arrested for 18 hours and stimulated with 10% fetal bovine serum (FBS) for 30 min. To appropriate samples, actinomycin D (10 μg/ml) was added and total RNA was harvested at specified time points. High Capacity cDNA (complementary DNA) kit (Applied Biosystems) was used for reverse transcription. PCR comprised SYBR Green PCR Master Mix (Applied Biosystems), mouse c-*jun* primers (5′-ACGGACCGTTCTATGACTGC-3′ and 5′-CCAGGTTCAAGGTCATGCTC-3′), and internal control GAPDH primers (5′-ACCACAGTCCATGCCATCAC-3′ and 5′-TCCACCACCCTGTTGCTGTA-3′). PCR cycles were as follows: 50°C for 2 min, 94°C for 10 min, and 30 cycles of 94°C for 30 s, 62°C for 30 s, and 72°C for 20 s. Triplicate reactions were analyzed on a Real-Time PCR Corbett Rotorgene machine. Fold changes were calculated by the method of ΔΔCt.

Tumor growth studies in mice

SCID (6- to 8-week-old) or C3H/HeN (8-week-old) mice were anesthetized with 1% isoflurane in oxygen and injected intradermally in the dorsal mid-back region with 1×10^6 T79 SCC cells/20 μl, 1.8×10^6 BCC-1/KMC cells/50 μl, or 1.8×10^6/50 μl UV13-1 cells in complete medium. Tumor-bearing mice were randomized before the initiation of treatment. Tumor volume was measured (length × height × width × π/6) with digital calipers before intratumoral administration of DNAzyme formulation. Tumor growth studies were performed with $n = 6$ to 8 mice per group.

Tumor cell metastasis to lung

T79 SCC cells, 12 hours after transfection with 0.4 μM Dz13 or Dz13scr, were injected (6×10^5 cells) into the tail veins of 8-week-old SCID mice. After 28 days, mice were killed and lung metastasis was quantified under a dissecting microscope.

Immunohistochemical analysis and flow cytometry

Solid tumors and metastatic lung tissues were fixed in 10% formalin and paraffin-embedded. Hematoxylin and eosin (H&E) and immunohistochemistry staining were performed with 4-μm sections. Immunohistochemical analysis was performed as previously described (*38*) with rabbit polyclonal antibodies sourced from Santa Cruz Biotechnology, BD Pharmingen, and GE Healthcare Life Sciences. Photomicrographs were taken at 200× or 400×. Staining density was quantified by counting the number of cells stained positive minimally "+" (where + = weak staining, ++ = moderate staining, +++ = strong staining) in three random fields per section (three separate sections per group) under magnification. The *y* axis represents the number of immunostained cells expressed as a percentage of the total number of cells per field. Apoptosis in cultured SCC was determined by annexin V staining and flow cytometry.

Oxidative stress analysis

Cells were incubated in the dark and at 37°C with 20 μM hydroethidine (Tyger Scientific) for 1 hour. Cells were washed with phosphate-buffered saline (PBS) and then scraped into 1 ml of PBS, counted, pelleted (200*g*, 10 min, 22°C), snap-frozen, and stored at −80°C until analysis. Cell lysates were extracted (80 μl of ice-cold 80% ethanol), mixed (1 min), and left on ice (20 min) in the dark. After centrifugation, the supernatant was subjected to LC-MS/MS analysis of hydroethidine and its oxidation products, $2OHE^+$ and E^+. Compounds were separated by LC on an Agilent 1290 Infinity UPLC (Agilent Technologies) with a Synergy Polar RP column (250 × 2.1 mm, Phenomenex) and a linear gradient of eluent A [H_2O containing 0.1% (v/v) formic acid] and eluent B [acetonitrile/H_2O, 90:10 (v/v), containing 0.1% (v/v) formic acid] as follows: 55 to 75% eluent B over 10 min, followed by an increase to 100% B over 2 min, a column wash with 100% B for 3 min, before returning to initial conditions (45% A, 55% B) for equilibration. The flow rate was 0.2 ml/min and the injection volume was 10 μl. The eluent from the column was then introduced into an Agilent 6460 A triple quadrupole mass spectrometer (Agilent Technologies) with the following settings: capillary voltage = 4.0 kV, gas temperature = 300°C, gas flow = 5 liters/min, nebulizer pressure = 20 psi, sheath gas heater = 350°C, sheath gas flow = 5 liters/min, drying gas = nitrogen, and the collision gas was ultrapure nitrogen (99.99%). Quantification of HE, $2OHE^+$, and E^+ was by multiple reaction monitoring mode with positive electrospray ionization MS and against authentic standards. For each analyte, the largest fragment ion generated by collision-induced dissociation of the $[M+H]^+$ ion was used for quantification. Settings for the target analytes were as follows (parent ion→fragment ion): HE mass/charge ratio (*m/z*) 316.2→210.1, $2OHE^+$ *m/z* 330.2→300, and E^+ *m/z* 314.2→285.1, with retention times of 5.5, 6.5, and 7.3 min, respectively.

c-Jun in tumors

Tumors were homogenized in complete protease inhibitor/PBS buffer (Roche, Complete Protease Inhibitor Cocktail Tablets) according to the manufacturer's instructions, and 20 μg was protein-resolved on 10% SDS–polyacrylamide gel electrophoresis (SDS-PAGE) gels alongside with increasing amounts of recombinant c-Jun protein (Active Motif). Polyvinylidene difluoride (PVDF) P membranes were incubated overnight with c-Jun antibodies (Abcam) at 4°C, followed by chemiluminescence detection with horseradish peroxidase–conjugated secondary antibodies. c-Jun protein was normalized to β-actin and quantified with National Institutes of Health ImageJ. Tumor c-Jun amounts were determined from the standard curve generated with recombinant c-Jun.

Zebrafish/tumor xenograft angiogenesis assay

The zebrafish/tumor xenograft angiogenesis assay was performed as described previously (*14*). Briefly, after trypsinization, T79 SCC cells were resuspended to 500 cells/μl with Matrigel and microinjected into the perivitelline space of Tg(fli1a:EGFP)^{y1} zebrafish embryos (*39*) at 48 hours after fertilization. Forty-eight hours after injection, tumor xenograft angiogenesis (sprouting from subintestinal vessel plexus) was observed under fluorescence microscopy (Olympus SZX16). Studies were performed with $n = 5$ per group.

c-*jun* mRNA expression in tumors

Tumors were placed into Lysing Matrix D tubes (FastPrep Sample Preparation System, Qbiogene) and homogenized in 1 ml of TRIzol reagent (*40*) with a Fastprep-24 Tissue and Cell Homogenizer (MP Biomedical) isolation of total RNA. cDNA was generated with SuperScript II and Oligo(dT) primer (Invitrogen) as per the manufacturer's instructions. c-*jun* mRNA was determined by quantitative real-time PCR.

Blood counts, coagulation, serum IFN-α and IL-6, and assessment of CD4$^+$ and CD8$^+$ populations

Whole blood was collected by cardiac puncture into tubes containing 3.8% sodium citrate at a ratio of five parts of blood to one part of sodium citrate. Hematologic measurements were done with a Coulter AT-diff Hematology Analyzer (Beckman Coulter). Peripheral blood mononuclear cells were isolated by density gradient centrifugation. Clotting times and tissue factor amounts were determined with a one-stage plasma recalcification test with a coagulometer (Diagnostica Stago) (*41*). Where indicated, mouse serum IFN-α or IL-6 was determined by ELISA (R&D Systems).

In the immunodepletion analysis, peripheral blood was collected by cardiac puncture, citrated, and combined with dextran solution. White cells were isolated in PBS (with 2% bovine serum albumin) and stained with CD8–fluorescein isothiocyanate, CD4-phycoerythrin, or isotype control IgG before the addition of 0.5% formaldehyde/1% sucrose/PBS and assessment of CD4$^+$ and CD8$^+$ cells by flow cytometry.

Toxicology studies in cynomolgus monkeys

A non–GLP-compliant pilot toxicology study was completed in cynomolgus monkeys before a GLP-compliant 28-day repeat-dose study. In the GLP-compliant repeat-dose study (Charles River Laboratories), cynomolgus monkeys were administered intravenous doses of Dz13/DOTAP/DOPE (0 to 180 μg of Dz13 per kilogram per day). Clinical signs, body weight, and food and water intake were monitored during the study; clinical biochemistry, hematology, and urinalysis parameters were assessed at completion of the study; and a necropsy with macroscopic organ observations, organ weight, and organ histological evaluation was completed at study conclusion. A nontreatment recovery period of 2 weeks was included in the study design.

Toxicology studies in Wistar rats

In a GLP-compliant study conducted at Harlan Laboratories, Wistar rats [HanRcc:WIST(SPF)] received Dz13/DOPE/DOTAP/DMEM by intradermal injection twice daily at four locations (total Dz13 dose of 800 μg) for a total of 4 days. The injection volume was 50 μl and contained 100 μg of Dz13. Control animals received DMEM only. At the end of the 7-day study period, all animals were killed and blood was collected for hematology and clinical biochemistry, necropsied, and examined post-mortem.

Pharmacologic analysis

Pharmacologic analysis for "off-target" activity was conducted by Ricerca Biosciences (formerly MDS Pharma Services) in which the median inhibitory concentration (IC_{50}) of Dz13 was evaluated in more than 70 separate enzyme-linked and radioligand-binding assays with nonlinear, least-squares regression analysis and MathIQ (ID Business Solutions). Alternatively, Hill coefficients (n_H) defining the slope of the competitive binding curve were calculated with MathIQ, and inhibition constants (K_i) were calculated with the equation of Cheng and Prusoff (*42*).

hERG analysis

GLP-compliant hERG analysis was performed with human embryonic kidney (HEK) 293 cells (stably expressing the hERG channel) using the whole-cell patch-clamp technique (bSys GmbH).

Local tolerance study

In a GLP-compliant local tolerance study conducted at Charles River Laboratories, three male Göttingen minipigs, aged 4 to 5 months, were dosed on days 1 and 4 by intradermal injection on the back region with sterile needles and plastic polypropylene syringes. Each animal received 50 μl of vehicle (DMEM), Dz13/DOPE/DOTAP (in DMEM), Dz13 alone (in DMEM), and DOPE/DOTAP alone (in DMEM) at different injection sites on two separate occasions (days 1 and 4) such that each animal received a total of eight injections. Injections were prepared immediately before administration. All animals were closely monitored during the study, clinical signs and food consumption were recorded daily, and body weight was recorded twice weekly. The study was terminated on day 7, the animals were necropsied, and all major organs and injection sites were collected and preserved in formalin. The injection sites were sectioned and stained with H&E and subjected to histological examination.

^{33}P-Dz13 plasma distribution study in rats

GLP-compliant plasma distribution analysis was conducted in male Sprague-Dawley rats (11 to 15 weeks) that received a single intravenous or intradermal administration of ^{33}P-Dz13/DOPE/DOTAP (Charles River Laboratories). Blood was collected at various times after administration into heparinized tubes, and the radioactivity in plasma was determined by liquid scintillation counting.

Biodistribution of ^{33}P-Dz13 in tumor-bearing mice

Dz13 (40 μg of Dz13 spiked with ^{33}P-Dz13) was injected intratumorally into T79 SCC tumor-bearing SCID mice, and after various times, the mice were killed; tumors, organs, and blood were collected; and radioactivity was assessed by liquid scintillation counting. Resected tumor was homogenized with TRIzol reagent (*40*) in Lysing Matrix D tube (BIO101), and DNA was extracted according to the manufacturer's instructions.

Statistical analysis

Statistical analysis was performed as stated in the text. Unless otherwise indicated, $^*P < 0.05$, and data were expressed as means ± SEM. Animal studies were approved by the University of New South Wales (UNSW) and Walter and Eliza Hall Institute (WEHI) Animal Care and Ethics Committees, or the Charles River Laboratories according to Animal Ethics guidelines as directed by the UK Home Office.

SUPPLEMENTARY MATERIALS

www.sciencetranslationalmedicine.org/cgi/content/full/4/139/139ra82/DC1

Table S1. Dz13/DOTAP/DOPE administration does not affect a range of hematologic and thrombotic parameters.

Table S2. Pharmacologic assessment of Dz13.

REFERENCES AND NOTES

1. U. Leiter, C. Garbe, Epidemiology of melanoma and nonmelanoma skin cancer—The role of sunlight. *Adv. Exp. Med. Biol.* **624**, 89–103 (2008).
2. C. S. Wong, R. C. Strange, J. T. Lear, Basal cell carcinoma. *BMJ* **327**, 794–798 (2003).
3. A. N. Crowson, Basal cell carcinoma: Biology, morphology and clinical implications. *Mod. Pathol.* **19** (Suppl. 2), S127–S147 (2006).
4. R. Bhindi, R. G. Fahmy, H. C. Lowe, C. N. Chesterman, C. R. Dass, M. J. Cairns, E. G. Saravolac, L. Q. Sun, L. M. Khachigian, Brothers in arms: DNA enzymes, short interfering RNA, and the emerging wave of small-molecule nucleic acid-based gene-silencing strategies. *Am. J. Pathol.* **171**, 1079–1088 (2007).

5. L. M. Khachigian, Catalytic DNAs as potential therapeutic agents and sequence-specific molecular tools to dissect biological function. *J. Clin. Invest.* **106**, 1189–1195 (2000).
6. S. W. Santoro, G. F. Joyce, A general purpose RNA-cleaving DNA enzyme. *Proc. Natl. Acad. Sci. U.S.A.* **94**, 4262–4266 (1997).
7. L. M. Khachigian, DNAzymes: Cutting a path to a new class of therapeutics. *Curr. Opin. Mol. Ther.* **4**, 119–121 (2002).
8. L. M. Khachigian, R. G. Fahmy, G. Zhang, Y. V. Bobryshev, A. Kaniaros, c-Jun regulates vascular smooth muscle cell growth and neointima formation after arterial injury. Inhibition by a novel DNA enzyme targeting c-Jun. *J. Biol. Chem.* **277**, 22985–22991 (2002).
9. E. Shaulian, M. Karin, AP-1 in cell proliferation and survival. *Oncogene* **20**, 2390–2400 (2001).
10. C. A. Sledz, M. Holko, M. J. de Veer, R. H. Silverman, B. R. Williams, Activation of the interferon system by short-interfering RNAs. *Nat. Cell Biol.* **5**, 834–839 (2003).
11. K. Kim, F. Liu, Inhibition of gene expression in human cells using RNase P-derived ribozymes and external guide sequences. *Biochim. Biophys. Acta* **1769**, 603–612 (2007).
12. G. M. Halliday, S. Le, Transforming growth factor-β produced by progressor tumors inhibits, while IL-10 produced by regressor tumors enhances, Langerhans cell migration from skin. *Int. Immunol.* **13**, 1147–1154 (2001).
13. G. Zhang, X. Luo, E. Sumithran, V. S. C. Pua, R. S. Barnetson, G. M. Halliday, L. M. Khachigian, Squamous cell carcinoma growth in mice and in culture is regulated by c-Jun and its control of matrix metalloproteinase-2 and -9 expression. *Oncogene* **25**, 7260–7266 (2006).
14. S. Nicoli, M. Presta, The zebrafish/tumor xenograft angiogenesis assay. *Nat. Protoc.* **2**, 2918–2923 (2007).
15. H. T. Yen, L. C. Chiang, K. H. Wen, C. C. Tsai, C. L. Yu, H. S. Yu, The expression of cytokines by an established basal cell carcinoma cell line (BCC-1/KMC) compared with cultured normal keratinocytes. *Arch. Dermatol. Res.* **288**, 157–161 (1996).
16. A. D. Lucas, G. M. Halliday, Progressor but not regressor skin tumours inhibit Langerhans' cell migration from epidermis to local lymph nodes. *Immunology* **97**, 130–137 (1999).
17. S. H. Jee, S. C. Shen, H. C. Chiu, W. L. Tsai, M. L. Kuo, Overexpression of interleukin-6 in human basal cell carcinoma cell lines increases anti-apoptotic activity and tumorigenic potency. *Oncogene* **20**, 198–208 (2001).
18. M. J. Cairns, T. M. Hopkins, C. Witherington, L. Q. Sun, The influence of arm length asymmetry and base substitution on the activity of the 10-23 DNA enzyme. *Antisense Nucleic Acid Drug Dev.* **10**, 323–332 (2000).
19. T. Uno, K. Takeda, Y. Kojima, H. Yoshizawa, H. Akiba, R. S. Mittler, F. Gejyo, K. Okumura, H. Yagita, M. J. Smyth, Eradication of established tumors in mice by a combination antibody-based therapy. *Nat. Med.* **12**, 693–698 (2006).
20. G. J. Weiner, H. M. Liu, J. E. Wooldridge, C. E. Dahle, A. M. Krieg, Immunostimulatory oligodeoxynucleotides containing the CpG motif are effective as immune adjuvants in tumor antigen immunization. *Proc. Natl. Acad. Sci. U.S.A.* **94**, 10833–10837 (1997).
21. S. Bauer, H. Wagner, Bacterial CpG-DNA licenses TLR9. *Curr. Top. Microbiol. Immunol.* **270**, 145–154 (2002).
22. M. M. Whitmore, M. J. DeVeer, A. Edling, R. K. Oates, B. Simons, D. Lindner, B. R. Williams, Synergistic activation of innate immunity by double-stranded RNA and CpG DNA promotes enhanced antitumor activity. *Cancer Res.* **64**, 5850–5860 (2004).
23. M. Hafner, R. Zawatzky, C. Hirtreiter, W. A. Buurman, B. Echtenacher, T. Hehlgans, D. N. Männel, Antimetastatic effect of CpG DNA mediated by type I IFN. *Cancer Res.* **61**, 5523–5528 (2001).
24. T. L. Roberts, M. J. Sweet, D. A. Hume, K. J. Stacey, Cutting edge: Species-specific TLR9-mediated recognition of CpG and non-CpG phosphorothioate-modified oligonucleotides. *J. Immunol.* **174**, 605–608 (2005).
25. *Estimating the Maximum Safe Starting Dose in Initial Clinical Trials for Therapeutics in Adult Healthy Volunteers* (Food and Drug Administration, Rockville, MD, 2005).
26. K. Rass, W. Tilgen, Treatment of melanoma and nonmelanoma skin cancer. *Adv. Exp. Med. Biol.* **624**, 296–318 (2008).
27. S. A. Rosenberg, N. P. Restifo, J. C. Yang, R. A. Morgan, M. E. Dudley, Adoptive cell transfer: A clinical path to effective cancer immunotherapy. *Nat. Rev. Cancer* **8**, 299–308 (2008).
28. B. Breart, F. Lemaître, S. Celli, P. Bousso, Two-photon imaging of intratumoral $CD8^+$ T cell cytotoxic activity during adoptive T cell therapy in mice. *J. Clin. Invest.* **118**, 1390–1397 (2008).
29. F. Ghiringhelli, L. Apetoh, A. Tesniere, L. Aymeric, Y. Ma, C. Ortiz, K. Vermaelen, T. Panaretakis, G. Mignot, E. Ullrich, J. L. Perfettini, F. Schlemmer, E. Tasdemir, M. Uhl, P. Génin, A. Civas, B. Ryffel, J. Kanellopoulos, J. Tschopp, F. André, R. Lidereau, N. M. McLaughlin, N. M. Haynes, M. J. Smyth, G. Kroemer, L. Zitvogel, Activation of the NLRP3 inflammasome in dendritic cells induces IL-1β–dependent adaptive immunity against tumors. *Nat. Med.* **15**, 1170–1178 (2009).
30. L. Apetoh, F. Ghiringhelli, A. Tesniere, M. Obeid, C. Ortiz, A. Criollo, G. Mignot, M. C. Maiuri, E. Ullrich, P. Saulnier, H. Yang, S. Amigorena, B. Ryffel, F. J. Barrat, P. Saftig, F. Levi, R. Lidereau, C. Nogues, J. P. Mira, A. Chompret, V. Joulin, F. Clavel-Chapelon, J. Bourhis, F. André, S. Delaloge, T. Tursz, G. Kroemer, L. Zitvogel, Toll-like receptor 4-dependent contribution of the immune system to anticancer chemotherapy and radiotherapy. *Nat. Med.* **13**, 1050–1059 (2007).
31. G. M. Halliday, A. Patel, M. J. Hunt, F. J. Tefany, R. S. Barnetson, Spontaneous regression of human melanoma/nonmelanoma skin cancer: Association with infiltrating $CD4^+$ T cells. *World J. Surg.* **19**, 352–358 (1995).
32. K. Rakhra, P. Bachireddy, T. Zabuawala, R. Zeiser, L. Xu, A. Kopelman, A. C. Fan, Q. Yang, L. Braunstein, E. Crosby, S. Ryeom, D. W. Felsher, $CD4^+$ T cells contribute to the remodeling of the microenvironment required for sustained tumor regression upon oncogene inactivation. *Cancer Cell* **18**, 485–498 (2010).
33. A. W. Griffioen, Anti-angiogenesis: Making the tumor vulnerable to the immune system. *Cancer Immunol. Immunother.* **57**, 1553–1558 (2008).
34. D. J. Betting, R. E. Yamada, K. Kafi, J. Said, N. van Rooijen, J. M. Timmerman, Intratumoral but not systemic delivery of CpG oligodeoxynucleotide augments the efficacy of anti-CD20 monoclonal antibody therapy against B cell lymphoma. *J. Immunother.* **32**, 622–631 (2009).
35. T. W. Wong, C. H. Chen, C. C. Huang, C. D. Lin, S. W. Hui, Painless electroporation with a new needle-free microelectrode array to enhance transdermal drug delivery. *J. Control. Release* **110**, 557–565 (2006).
36. L. M. Khachigian, D. A. Owensby, C. N. Chesterman, A tyrosinated peptide representing the alternatively spliced exon of the platelet-derived growth factor A-chain binds specifically to cultured cells and interferes with binding of several growth factors. *J. Biol. Chem.* **267**, 1660–1666 (1992).
37. L. A. Rafty, L. M. Khachigian, Zinc finger transcription factors mediate high constitutive platelet-derived growth factor-B expression in smooth muscle cells derived from aortae of newborn rats. *J. Biol. Chem.* **273**, 5758–5764 (1998).
38. G. Zhang, C. R. Dass, E. Sumithran, N. R. Di Girolimo, L.-Q. Sun, L. M. Khachigian, Effect of deoxyribozymes targeting c-Jun on solid tumor growth and angiogenesis in rodents. *J. Natl. Cancer Inst.* **96**, 683–696 (2004).
39. N. D. Lawson, B. M. Weinstein, In vivo imaging of embryonic vascular development using transgenic zebrafish. *Dev. Biol.* **248**, 307–318 (2002).
40. R. Sungaran, O. T. Chisholm, B. Markovic, L. M. Khachigian, Y. Tanaka, B. H. Chong, The role of platelet α-granular proteins in the regulation of thrombopoietin messenger RNA expression in human bone marrow stromal cells. *Blood* **95**, 3094–3101 (2000).
41. H. Cai, C. Song, I. G. Lim, S. A. Krilis, C. L. Geczy, H. P. McNeil, Importance of C-reactive protein in regulating monocyte tissue factor expression in patients with inflammatory rheumatic diseases. *J. Rheumatol.* **32**, 1224–1231 (2005).
42. Y. Cheng, W. H. Prusoff, Relationship between the inhibition constant (K_1) and the concentration of inhibitor which causes 50 per cent inhibition (I_{50}) of an enzymatic reaction. *Biochem. Pharmacol.* **22**, 3099–3108 (1973).

Acknowledgments: We thank N. McLaughlin and S. Rana for excellent technical assistance, C. Power for helpful advice, and A. Au-Yeung for critical reading of the manuscript. We also thank M. J. Smyth (Peter MacCallum Cancer Centre, Australia) for supplying CD4 and CD8 antibodies. **Funding:** Supported by a Translational Program Grant from Cancer Institute of New South Wales, with additional support from National Health and Medical Research Council (NHMRC), Australia Research Council, and Cancer Council of New South Wales. **Author contributions:** L.M.K. designed, directed, and analyzed all aspects of this research; R.S., C.R.P., B.H.C., G.J.L., T.-W.W., C.N.C., D.J.F., F.J.M., R.S.C.B., and G.M.H. directed various elements in the study or provided critical material and intellectual input; H.C., F.S.S., L.P.-L., B.W., M.P., M.P.D., and G.J.M. performed the work and analyzed the data. L.M.K. is an Australia Fellow of the NHMRC. **Competing interests:** NewSouth Innovations Pty Ltd., the commercialization arm of UNSW, has intellectual property interests in Dz13 and has applied for a U.S. patent (application #10/923197) entitled "Vascular therapeutics" on which L.M.K. is an author. None of the other authors declare any competing interests.

Submitted 1 March 2012
Accepted 12 April 2012
Published 20 June 2012
10.1126/scitranslmed.3003960

Citation: H. Cai, F. S. Santiago, L. Prado-Lourenco, B. Wang, M. Patrikakis, M. P. Davenport, G. J. Maghzal, R. Stocker, C. R. Parish, B. H. Chong, G. J. Lieschke, T.-W. Wong, C. N. Chesterman, D. J. Francis, F. J. Moloney, R. S.C. Barnetson, G. M. Halliday, L. M. Khachigian, DNAzyme targeting *c-jun* suppresses skin cancer growth. *Sci. Transl. Med.* **4**, 139ra82 (2012).